Shock Waves (2013) 23:559–573
DOI 10.1007/s00193-013-0467-2

ORIGINAL ARTICLE

Numerical models for afterburning of TNT detonation products in air

L. Donahue · F. Zhang · R. C. Ripley

Received: 17 December 2012 / Revised: 9 May 2013 / Accepted: 11 August 2013 / Published online: 1 September 2013

Abstract Afterburning occurs when fuel-rich explosive detonation products react with oxygen in the surrounding atmosphere. This energy release can further contribute to the air blast, resulting in a more severe explosion hazard particularly in confined scenarios. The primary objective of this study was to investigate the influence of the products equation of state (EOS) on the prediction of the efficiency of trinitrotoluene (TNT) afterburning and the times of arrival of reverberating shock waves in a closed chamber. A new EOS is proposed, denoted the Afterburning (AB) EOS. This EOS employs the JWL EOS in the high pressure regime, transitioning to a Variable-Gamma (VG) EOS at lower pressures. Simulations of three TNT charges suspended in a 26 m^3 explosion chamber were performed. When compared to numerical results using existing methods, it was determined that the Afterburning EOS delays the shock arrival times giving better agreement with the experimental measurements in the early to mid time. In the late time, the Afterburning EOS roughly halved the error between the experimental measurements and results obtained using existing methods. Use of the Afterburning EOS for products with the Variable-Gamma EOS for the surrounding air further significantly improved results, both in the transient solution and the quasi-static pressure. This final combination of EOS and mixture model is recommended for future studies involving afterburning explosives, particularly those in partial and full confinement.

Keywords Afterburning · TNT · Confined explosion · Explosive blast · Numerical modelling · Equation of state

Communicated by C. Needham.

L. Donahue (✉) · R. C. Ripley
Martec Limited, Suite 400, 1888 Brunswick St., Halifax, NS B3J 3J8, Canada
e-mail: laura.donahue@lr.org

R. C. Ripley
e-mail: robert.ripley@lr.org

F. Zhang
Defence Research and Development Canada - Suffield, PO Box 4000, Station Main, Medicine Hat, AB T1A 8K6, Canada
e-mail: fan.zhang@drdc-rddc.gc.ca

1 Introduction

The primary source of energy release available in a high explosive comes during the detonation process, which has an energy release timescale on the order of microseconds. High explosives are generally CHNO molecules, and the resulting detonation products typically consist of a range of chemical species, including CO_2, H_2O, N_2, O_2 (in the case of oxygen-rich explosives), C, CO, H_2, and a variety of hydrocarbons. The products can be fuel rich, fuel lean, or balanced, depending on the explosive formulation.

In the case of fuel-rich explosives such as trinitrotoluene (TNT, $C_7H_5N_3O_6$), a second energy release mechanism exists. Afterburning [1] occurs when species in the detonation products, such as carbon and carbon monoxide, mix and react with oxidizers in the surrounding atmosphere. Unlike detonation, afterburning is a late-time combustion process which occurs on a timescale on the order of milliseconds to seconds. Complete combustion of these residual fuels will produce an added energy equal to approximately twice the detonation energy in the case of TNT. This additional energy can contribute to the air blast, resulting in a more severe explosion hazard. Afterburning takes place efficiently only when the detonation products are well mixed

with the surrounding air and under appropriate combustion conditions.

TNT explosion performance has been studied experimentally in both free-field configurations (unconfined) and closed vessels (full confinement). The concept of afterburning was suggested by Dewey [1] in the 1950s who found the decay in velocity behind the shock wave from a large-scale unconfined TNT explosion differed significantly from the standard Freidlander form [2]. Dewey then confirmed this hypothesis through further experiments involving a high oxygen-balance explosive. Ornellas investigated afterburning phenomena using small-scale bomb calorimeter experiments [3], while Wolanski [4] visualized the combustion of small-scale TNT explosions and observed a more pronounced reaction in the presence of oxygen-enriched air. Zhang et al. [5] and Kuhl et al. [6] studied the afterburning effect for high explosives in larger-scale fully confined explosions.

Other researchers have gained insight into the afterburning phenomenon using numerical and analytical techniques. Kuhl et al. have proposed a thermodynamic model for explosive afterburning [6–8], whereby a Le Chatelier diagram (internal energy vs. temperature) is used to describe the component fits and the afterburning combustion process. The Jones–Wilkins–Lee (JWL) EOS is employed in the high-pressure regime (out to an expansion of 3 charge radii [8]), with the quadratic thermodynamic model used at lower pressures with good results. Ames et al. have presented an analytical method by which the relative levels of detonation and afterburning energy release in a confined explosion can be determined based on detailed pressure-time histories [9].

The current work focuses on numerical afterburning investigations, specifically using computational fluid dynamic (CFD) methods. Appropriate prediction of the magnitudes and arrival times of shock or pressure waves in a confined explosion scenario is challenging to all numerical codes in part due to the interdependence of shock wave propagation and thermodynamic state. Previous simulations of blasts in a large explosion chamber [10] have shown that in the early time, shocks of the correct magnitude were predicted; however, waves arrived sooner than in the experiments. At late times, there were differences in both the shock arrival times and the quasi-static pressure (QSP). Discrepancies can be attributed to several factors including afterburning reaction schemes, turbulent mixing, and equations of state.

The influence of the products EOS on the prediction of the efficiency of TNT afterburning and the times of arrival of reverberating shock waves in a closed chamber is presented here. A new EOS is given for more effective simulation of afterburning explosive products. Comparison to large-scale experimental data is used to quantify the results. This paper is partially based on studies given in [11,12].

2 Platform for model development

All new and existing models used in this work are designed for a finite volume computational fluid dynamics framework, specifically the Chinook CFD code developed by Martec Limited. Chinook has been validated against a wide range of analytical and experimental solutions involving shock and blast. The code employs an explicit time-stepping approach to solve the Euler equations for mass, momentum, and energy [13] with second-order spatial accuracy. When solving for multiple materials and chemical species, an additional equation is solved for each material/specie.

The HLLC flux solver of Harten, Lax, and van Leer [14] is used in the explicit solution to the Euler equations. Due to the exact resolution of contact waves, the HLLC scheme is ideally suited for compressible multiple material solutions, and was used throughout this study.

2.1 Equations of state

Chinook contains equations of state relevant to TNT detonation and explosion modeling including JWL for the detonation products, Mie–Gruneisen for the condensed unreacted explosive, and a Shocked-Air (CEA) EOS for the surrounding atmosphere. These equations of state are detailed in the following sections.

In the present simulations, mixtures of materials are handled using a continuum approach. Mixtures of materials in a computational cell are assumed to be in mechanical (pressure and velocity) equilibrium with a mixed sound speed and temperature, following the approach of Benson [15].

2.1.1 Mie–Gruneisen equation of state

The Mie–Gruneisen equation of state (EOS) is used to describe the behaviour of the condensed-phase unreacted explosive. The coefficients for this EOS are based on fitting functions from experimental data. This equation is described in detail in [16], where it forms the condensed-phase portion of the HOM EOS. The shock Hugoniot temperature is computed as described in the HOM EOS, and using fits to Walsh and Christian data [16].

2.1.2 JWL equation of state

Two forms of the JWL EOS are commonly used to model the expansion of detonation products from high explosives, assuming no heat loss to the surroundings. The JWL EOS is an empirical relationship that was formulated by Lee et al. [17] following earlier equations of state proposed by Jones and Miller [18] and Wilkins [19], and can be expressed in isentropic form as:

$$P = Ae^{-R_1 V} + Be^{-R_2 V} + CV^{-(\omega+1)}, \quad (1)$$

where P is the pressure, and A, B, C, R_1, R_2, and ω are constants. V is the relative volume equal to ρ_o/ρ, with ρ being the density and the subscript o representing a reference value. This EOS can also be written in terms of energy [17] by integrating the isentropic relation $\mathrm{d}e/\mathrm{d}v = -P$ [20]:

$$P = A\left(1 - \frac{\omega}{R_1 V}\right)e^{-R_1 V} + B\left(1 - \frac{\omega}{R_2 V}\right)e^{-R_2 V} + \frac{\omega \rho_o e}{V} \quad (2)$$

where e is the specific internal energy.

Several sets of JWL EOS constants are given in the literature (such as in the review by Dobratz [21]); however, constants can also be calculated using the Cheetah thermochemical equilibrium code [22,23]. The Cheetah 2.0 JWL parameters for TNT with an initial density of 1,600 kg/m^3 are listed in Table 1, calculated using the bkwc product library and a composition freeze temperature of 1,800 K [24].

2.1.3 Shocked-Air (CEA) equation of state

The Shocked-Air (CEA) EOS was developed by Martec in response to the need for a simple EOS for air with better predictions of shocked pressures and temperatures than the ideal gas EOS with a fixed specific heat ratio [25]. A curve fit for specific heat ratio as a function of internal energy was extracted from CEA (Chemical Equilibrium with Applications [26]) data for air at different pressures and temperatures. This internal energy-dependent specific heat ratio is then used with the Ideal Gas EOS to yield more accurate shocked state properties.

2.2 Detonation modelling

Using the Cheetah code, the specific detonation product species and their relative concentrations were determined from a point on the adiabat after the composition was frozen. The composition was chosen at this point as opposed to a higher-pressure state as afterburning reactions tend to occur predominantly after considerable expansion of the products. The following composition was extracted from the Cheetah equilibrium analysis, neglecting all but the primary species and ensuring that the reaction equation was balanced by normalizing the Cheetah values:

$$C_7H_5N_3O_{6(s)} \rightarrow 2.2CO_{(g)} + 1.6H_2O_{(g)} + 1.5N_{2(g)} + 1.1CO_{2(g)} + 0.36H_{2(g)} + 0.27CH_{4(g)} + 3.43C_{(s)} \quad (3)$$

The specific heat of detonation calculated for this reduced reaction is 4.47 MJ/kg-TNT. This is in good agreement with the Cheetah full equilibrium calculation, which also includes H_3N, C_2H_4, CH_2O_2, CH_2O, C_2H_6, CH_3OH, CH_3, NO, O_2, and NO_2 (4.495 MJ/kg-TNT), and the experimental detonation energy range of 4.409–4.573 MJ/kg-TNT found by Ornellas [3].

The detonation is modeled using a constant reaction time model which converts unreacted explosive material into detonation products with a specific heat release and rate. The reaction can only proceed once a user-defined ignition temperature has been exceeded. The constant reaction time model is a macro-scale model, and as such the detonation reaction zone is not resolved. However, the model is capable of capturing the CJ state and detonation velocity, while releasing the appropriate user-defined detonation energy. This model is useful in large-scale explosive blast and late-time analyses where phenomena such as detonation failure do not need to be predicted.

Chemical species are created behind the detonation front in the relative concentrations given by the detonation chemical reaction. These chemical species obey conservation and advection laws, and are used to track the flow of the different afterburning fuels and resulting combustion products throughout the domain.

2.3 Afterburning modelling

To model the afterburning energy release, a series of afterburning reactions are specified with their associated heats of reaction, ΔH_r, and ignition temperatures, T_ig, as shown

Table 1 JWL parameters for TNT ($\rho_o = 1{,}600$ kg/m^3) calculated from Cheetah 2.0

Parameter	Value
A (GPa)	493.633
B (GPa)	5.962
C (GPa)	1.199
R_1	4.749
R_2	1.057
ω	0.300

Table 2 Afterburning model parameters

Chemical formula	Model parameters
$CO + 0.5O_2 \rightarrow CO_2$	$\Delta H_\mathrm{r} = 10.1$ MJ/kg-CO
	$T_\mathrm{ig} = 880$ K
$H_2 + 0.5O_2 \rightarrow H_2O$	$\Delta H_\mathrm{r} = 120.9$ MJ/kg-H_2
	$T_\mathrm{ig} = 850$ K
$C + O_2 \rightarrow CO_2$	$\Delta H_\mathrm{r} = 32.8$ MJ/kg-C
	$T_\mathrm{ig} = 975$ K
$CH_4 + 2O_2 \rightarrow CO_2 + 2H_2O$	$\Delta H_\mathrm{r} = 50.0$ MJ/kg-CH_4
	$T_\mathrm{ig} = 850$ K

in Table 2. Chemical species are created by the detonation model in the case of the detonation products, and air is initialized with the appropriate levels of N_2 and O_2. When fuel and oxidizer species are detected simultaneously in a computational cell and the temperature exceeds the ignition temperature, the fuel and oxidizer species react in stoichiometric proportions. Using governing equation source terms, the fuel and oxidizer species are removed from the cell and the product species are created, conserving mass. The given heats of reaction are accounted for in a source term on the governing equation for energy to account for the transformation of chemical potential energy (not explicitly modeled) to internal energy (modeled quantity). These reactions are assumed to be controlled by in-cell mixing and to progress with an infinite reaction rate (instantaneous reaction) as in [6], and in the forward direction only.

3 TNT explosion in a closed chamber

Experiments involving confined TNT explosions in an air environment have been conducted at Defence R & D Canada-Suffield [5] and are used for comparison with the numerical methods. Charges were suspended in the centre of a 26 m^3, 3 m I.D., 4.2 m long closed explosion chamber, shown in Fig. 1. Five pressure transducers (P1, P2, P3, P5, and P9) were mounted along the inner chamber wall as shown in the figure. While P1, P2 and P3 were on the front side at 0.762-m intervals and 0.254 m above the horizontal mid plane, P9 was located on the opposite side of P2, 0.254 m below the horizontal mid plane. Gauge P5 was at the end of the chamber. Experimental data involving 1.1, 2.2, and 4.0 kg uncased, cylindrical TNT charges were used to study the effect of EOS on the transient and quasi-static pressure results. All charges had a diameter-to-height ratio of approximately 1.0 with a density of roughly 1,600 kg/m^3. The charges were suspended vertically at the centre of the explosion chamber and initiated at the top end by a RP83 detonator.

All numerical simulations in the study were executed in two steps. The explosive initiation, detonation propagation, initial fireball expansion, and transition to air blast were simulated on an axi-symmetric, two-dimensional (2D) unstructured mesh (approx. 870,000 cells, 1–5 mm cell size). The 2D results were then used to initialize a half-symmetric (along chamber length), three-dimensional, unstructured, boundary-fitted mesh (approx. 4.7 million cells, 25.4 mm cell size) at a time prior to the blast wave interaction with the chamber wall. A schematic of the charge position/orientation in the half-symmetric, three-dimensional computational domain is given in Fig. 2. A grid convergence study was performed to ensure that appropriate computational mesh resolutions were employed. The ambient chamber conditions in each simulation were set to the field-measured values from the appropriate experimental trial (typically around 280 K and 93 kPa).

Figure 3 shows a comparison between the experimental measurements and the baseline numerical results obtained using a standard JWL EOS (2) for the detonation products and the CEA EOS for the air. The overall shock structure shown in the pressure- and impulse-history is typical of those found in fully confined explosions. The initial shock arrival is characterized by a relatively high-magnitude discontinuity with a rapid decay to near-ambient pressures. The subsequent waves become far more complex, and it becomes difficult to identify and track the path of specific waves (first reflection, second reflection, etc). As the shocks continue to reflect and interact within the chamber, the wall pressure ceases to decay to the same extent and there is an overall increase in the overall chamber pressure. In the late time, a single low frequency oscillation is prevalent which is a function of the chamber dimensions and the sound speed of the resulting explosion product mix. The mean pressure about which this fluctuation occurs is known as the quasi-static pressure.

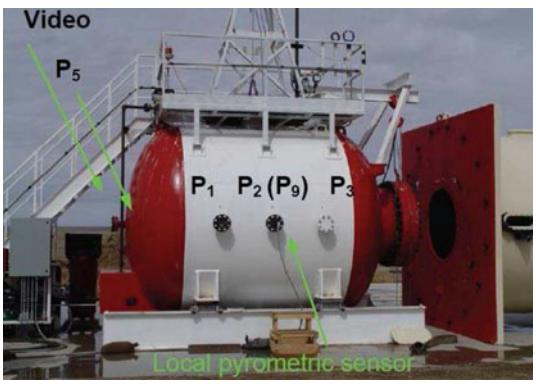

Fig. 1 DRDC Suffield explosion chamber gauge locations

Fig. 2 Schematic of computational domain and charge position

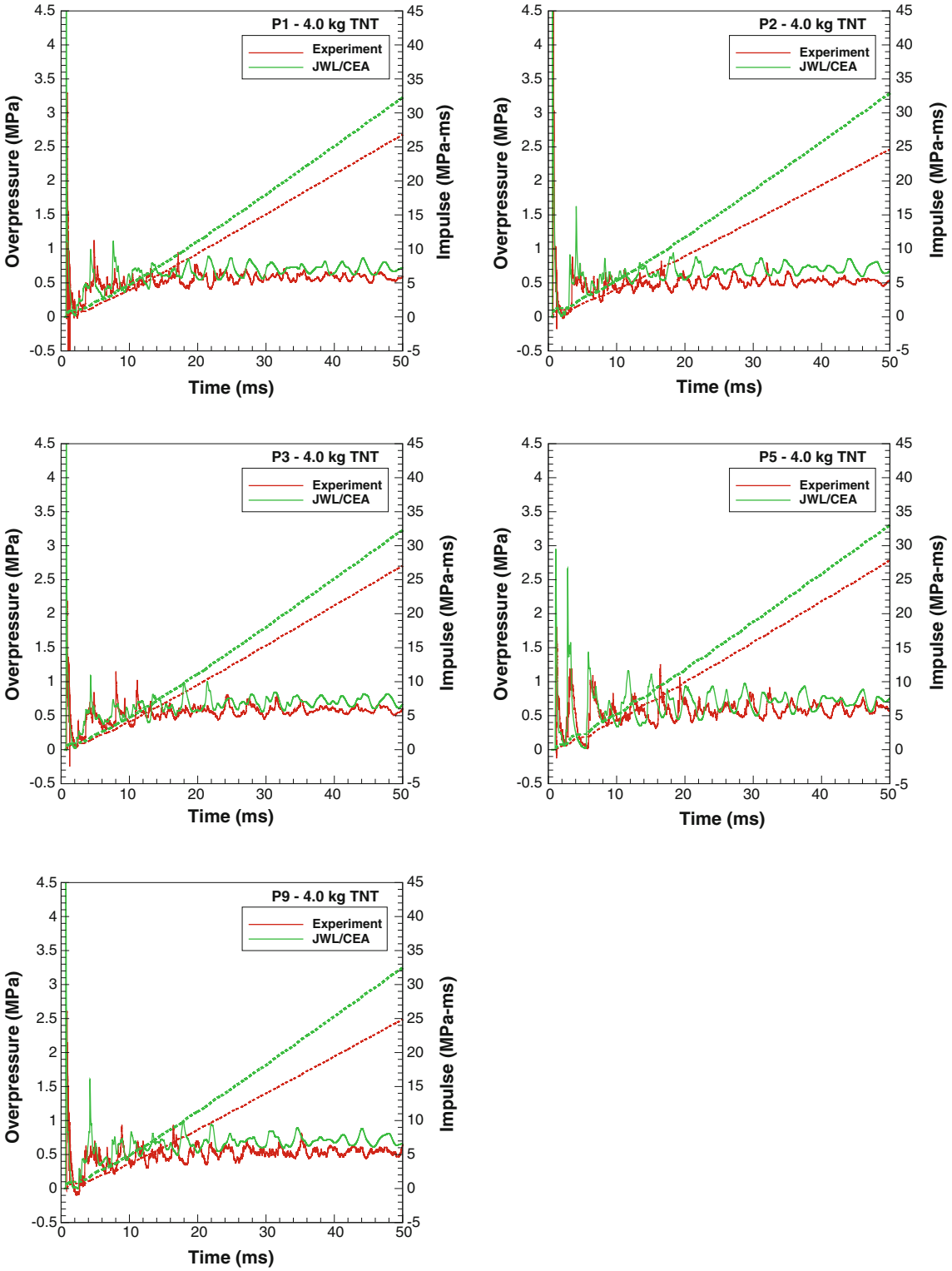

Fig. 3 Comparison of baseline simulation results (JWL/CEA) with experiment for 4.0 kg TNT scenario (*solid lines* pressure, *dashed lines* impulse)

Figure 3 shows an example of poor agreement between numerical and experimental results. While the overall numerical shock structure given in Fig. 3 does bear some resemblance to the measured values, there is disagreement in shock arrival times beginning at around 4 ms, with significant differences in the transient solution evident after 10 ms. The

numerical models also significantly over-predict the late-time quasi-static pressure. There are several possible sources of error which may explain this discrepancy. Simulations of closed chambers are relatively well defined with few unknowns. Differences in quasi-static pressure could be due to (1) incorrect amount of explosive energy release or (2) incorrect state calculation from conserved quantities. The energy released in detonation is relatively well quantified; hence the two numerical models which may arguably have the largest impact on these results are the equations of state used and the afterburning model.

Considering the equations of state being employed in this simulation, the JWL EOS, used to solve for the detonation- and afterburning-products thermodynamic state, has the highest potential for error. As discussed in Sect. 2.1.2, the JWL EOS is a very useful EOS for the simulation of explosive detonation products; the EOS coefficients are based on the expansion of detonation products in the absence of afterburning. However, afterburning can result in substantial changes in products composition which are not reflected in the JWL EOS coefficients. The need for an EOS which accounts for changes in composition due to afterburning is the primary issue driving the research described in this paper.

4 Afterburning equation of state theory

A new EOS, denoted the Afterburning (AB) EOS, was developed to take changes in composition during afterburning into account in the calculation of primitive variables (pressure, soundspeed, etc.). The Afterburning EOS is a combination of two other equations of state, JWL and Variable Gamma, with a smoothing function to transition between the two.

4.1 JWL equation of state parameter study

The JWL EOS is practical and very commonly used in the simulation of the early time, high-pressure product expansion such as arising from explosive detonation. The locus of TNT product expansion states, as calculated by the C-form JWL EOS (1), is given in Fig. 4 for pressure as a function of the relative volume. The analysis of the energy form of the EOS (2) gives the same results, although the calculation is more complex due to the presence of the energy term. The symbols show the states calculated by Cheetah and used in the equation fit. The contributions of each of the three right-hand-side terms of Eq. 1 are plotted, labeled *A term*, *B term*, and *C term*, respectively. As illustrated in Fig. 4, the A and B terms contribute only to the low relative-volume/high-pressure regime, while the final term is most significant at more expanded states. The final term in the energy form of the JWL EOS (2) is essentially the isentrope in the Ideal Gas EOS with the constant $\omega = \gamma - 1$, where γ (gamma) is the specific heat ratio [17]. The energy-dependent form of the EOS is used in this work.

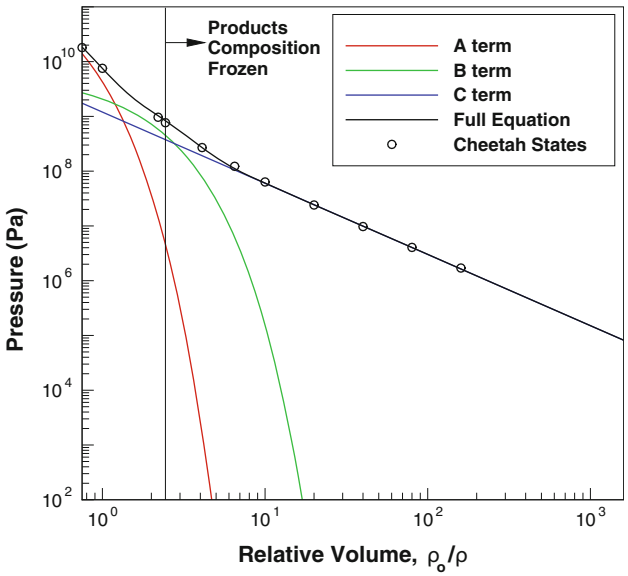

Fig. 4 Relative strengths of JWL terms in TNT products expansion

4.2 Variable-Gamma equation of state

The JWL EOS only describes the isentropic expansion of the closed system of detonation products and does not take afterburning into account (constant-gamma assumption). Most afterburning occurs at relatively low pressures (< 100 atm compared with detonation pressures of 180,000 atm) where the Ideal Gas EOS can be used with confidence. Therefore, to model the late-time, lower-pressure combustion, a Variable-Gamma (VG) EOS is employed. The effect of spatial and temporal changes in composition is accounted for by calculating the specific heat ratio of the mixture of chemical species in each computational cell at each timestep, as opposed to utilizing a constant value. The resulting variable gamma is used in the Ideal Gas EOS.

To compute the combustion product specific heat ratio, a polynomial equation and coefficients from the Cheetah 2.0 code are used. The specific heat at constant pressure, C_p, is determined by first calculating [22]:

$$\frac{\widetilde{C}_{pi}}{R} = C_1 + C_2\theta + C_3\theta^2 + C_4\theta^3 + C_5\theta^{-1} + C_6\theta^{-2} + C_7\theta^{-3} \quad (4)$$

where R is the universal gas constant, C_n are the polynomial fits given in the Cheetah code, and θ is equal to $Tx10^{-3}$, with T being the temperature in degrees Kelvin. Temperature is computed iteratively in the first computational timestep, and the temperature from the previous iteration is used in all subsequent steps. The subscript i refers to the specific

component species, with each species having a separate set of fit coefficients, and the ~ denotes a molar quantity.

The mixed specific heat at constant pressure is calculated according to:

$$(C_p)_{\text{mix}} = \sum_{i=1}^{n_{\text{gas}}} \frac{\widetilde{C}_{pi} Y_i}{W_i}, \tag{5}$$

where Y is the mass fraction and W is the molecular weight. The specific heat at constant volume, C_v, is then calculated by:

$$(C_v)_{\text{mix}} = \sum_{i=1}^{n_{\text{gas}}} \frac{(\widetilde{C}_{pi} - R) Y_i}{W_i} + \sum_{j=1}^{n_{\text{cond}}} \frac{\widetilde{C}_{pj} Y_j}{W_j} \tag{6}$$

In the current work, condensed products such as carbon are included as part of the fluid phase, i.e. a separate particulate phase is not simulated. However, the distinction between gas species and condensed species must be made as $C_p = C_v$ for condensed materials. Finally, the specific heat ratio is:

$$\gamma = \frac{(C_p)_{\text{mix}}}{(C_v)_{\text{mix}}} \tag{7}$$

This mixed specific heat ratio is used with the Ideal Gas EOS ($P = \rho e(\gamma - 1)$) to obtain species- and temperature-dependent fluid quantities.

The treatment of condensed species in the detonation products is accounted for in the Variable-Gamma EOS by setting $C_p = C_v$ as opposed to modeling a separate phase. A simple analysis shows that the amount of condensed products in the chamber is very small. For the 4.0 kg charge, a total of 0.725 kg of solid carbon is created (based on the assumed composition given in Sect. 2.2), which represents approximately 18% of the charge by mass. Carbon occurs in high concentrations during the initial expansion. During this time, the JWL EOS is used which takes solid carbon into account. Considering expansion into the entire chamber volume, the concentration of solid carbon is 0.0279 kg/m^3, or 2% of the total concentration (1.331 kg/m^3). At this low level, the effect of including condensed products in the fluid phase should be small.

4.3 Equation of state transition

To use the Variable-Gamma EOS in combination with the JWL EOS to model the pressure during initial products expansion as well as later-time afterburning, two density limits are specified. At densities above the upper limit, ρ_U, the JWL EOS is used, while the Variable-Gamma EOS is employed at densities below the lower limit, ρ_L. For densities within the intermediate range, a simple smoothing function is used to transition between the two equations of state. The transition function is summarized below, with the variable x representing one of the variables calculated using the EOS (pressure, temperature, soundspeed).

$$\begin{aligned}
&\text{for} \quad \rho \geq \rho_U \qquad x = f(\text{JWL}) \\
&\text{for} \quad \rho_L < \rho < \rho_U \begin{cases} x_{\text{JWL}} = f(\text{JWL}) \\ x_{\text{VG}} = f(\text{VG}) \\ x = \dfrac{x_{\text{JWL}} - x_{\text{VG}}}{\rho_U - \rho_L}(\rho - \rho_L) + x_{\text{VG}} \end{cases} \\
&\text{for} \quad \rho \leq \rho_L \qquad x = f(\text{VG})
\end{aligned} \tag{8}$$

In the current work, an upper density limit of 200 kg/m^3 and a lower density limit of 160 kg/m^3 are employed. The upper limit corresponds to a B-term value of 10 atm, while the lower limit corresponds to a B-term value of 1 atm (see Fig. 5). These values were selected because at these densities, the contributions of the high-pressure A and B terms do not significantly contribute to the overall pressure. The upper- and lower-density limits correspond to charge expansions of $2R_c$ and $2.15R_c$, respectively, for an equivalent spherical charge. This is less than the value of $3R_c$ used by Bell et al. for the transition from the JWL EOS in their work [8]. For a 4.0 kg spherical charge, these upper and lower expansion limits correspond to physical fireball radii of approximately 0.168 and 0.181 m. Given that the chamber radius is 1.5 m, the transition between equations of state occurs very quickly (over an expansion of 1.3 cm), and well before the shock or fireball interacts with the chamber walls.

The smoothing range employed in this work is necessary as instantaneously switching between equations of state at a singular density value causes discontinuities in pressure and sound speed. With this linear smoothing method,

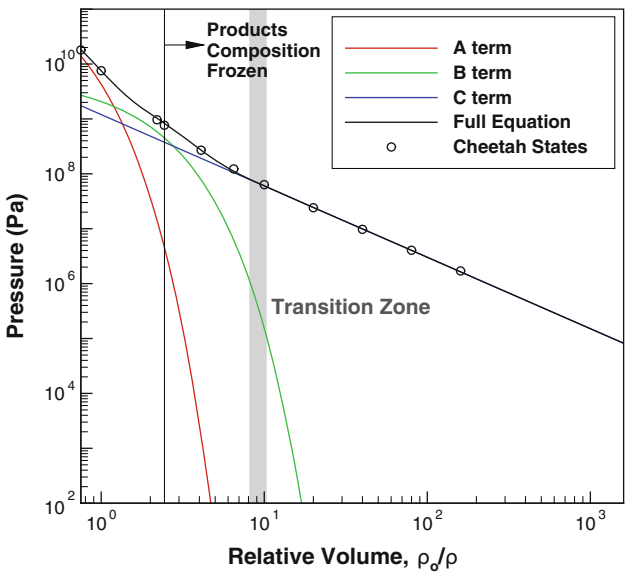

Fig. 5 Afterburning EOS transition zone for TNT

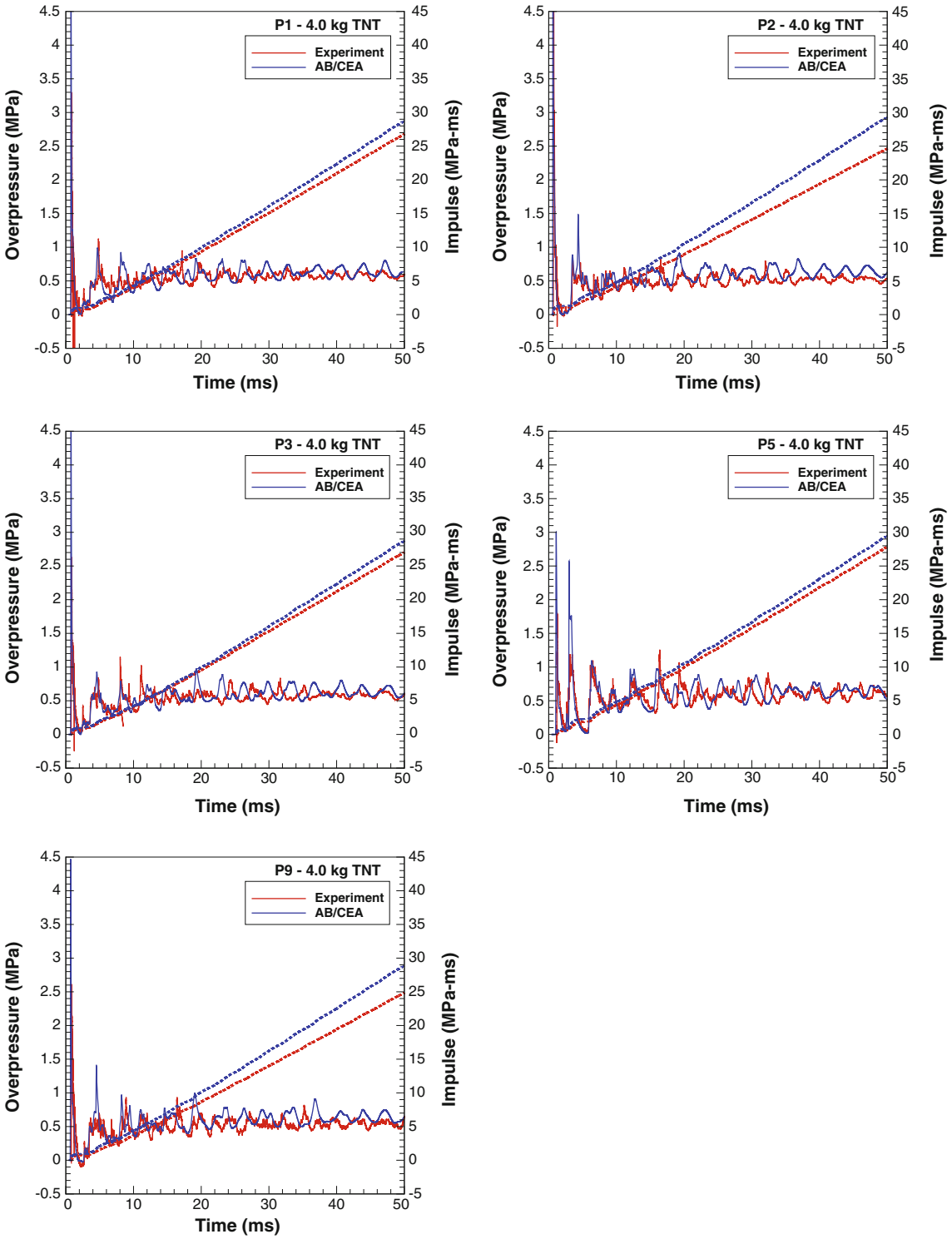

Fig. 6 Comparison of simulation results using Afterburning EOS (AB/CEA) with experiment for 4.0 kg TNT scenario (*solid lines* pressure, *dashed lines* impulse)

the pressure, sound speed and temperature computed with the two EOSs may not be consistent with each other. However,because the transition occurs so quickly and at such an early time, and also because the transition function does not affect any conserved quantities, the potential effect on the end results is very small.

5 Effect of detonation products equation of state

Figure 6 illustrates the results obtained when using the new Afterburning EOS in place of the JWL EOS for the detonation products. The experimental measurements are also shown for comparison. The Afterburning EOS results in better agreement in the early time shock arrival times, improved waveform agreement up to 15 ms, and a lower late-time quasi-static pressure, as compared with the JWL EOS alone. However, there are still substantial differences in the transient solution after 10 ms, and the quasi-static pressure continues to over-predict the experimental value as evidenced by the differences in the slope of the impulse.

6 Effect of air equation of state and mixing model

Although there are some detailed physical models in use in computational codes, all models can only give approximations to real-world physics and there is inherently some associated degree of error. The late-time solution is dominated by the air and afterburning product equations of state and the mixing model. Therefore, the overall analysis was simplified to reduce the number of models used in the simulation and hopefully the associated cumulative model inaccuracy as well.

As opposed to using the CEA EOS for the air, the Variable-Gamma EOS from the Afterburning EOS was employed. During the very-early time products expansion when the Afterburning EOS is dominated by the JWL EOS, the air and product materials are mixed using the existing mixing model based on a continuum approach. However, when the Afterburning EOS transitions to Variable-Gamma mode, quantities of all individual chemical species in the cell (products and air) are used to compute a single mixed specific heat ratio. The determination of which mixing method to use is made automatically at each numerical timestep and in each computational cell.

Figure 7 gives a comparison between the experimental measurements and numerical results (AB/VG) obtained using this new approach. Visually, there appears to be far better agreement in both the transient solution and the quasi-static pressure than in either of the previous results (Figs. 3, 6). At most gauge locations, the transient solution shows very good agreement up to about 10 ms, and the frequency and quasi-static pressure in the late time also compare quite well.

Simulations of other TNT explosive masses were conducted to determine if this technique also provided good agreement for other loading densities (ratio of explosive mass to chamber volume). Select results are given in Fig. 8 for 1.1 and 2.2 kg explosive masses, and pressure histories at the P2 and P5 locations. These gauge locations were selected as they are closest to being in the centre and the end of the chamber, respectively. The trends observed in the 4.0 kg simulations are retained here, with good agreement in both the transient and quasi-static pressures. The P5 gauge shows the greatest level of late-time transient variation, which is not unexpected. The blast at this location is especially challenging to predict due to the placement of the gauge near the rounded end of the chamber which is subject to considerable wave focusing of complex shock patterns.

7 Quantitative comparison of model performance

Earlier comparisons between experimental and numerical results focused on qualitative, apparent visual differences between pressure- and impulse-time history plots. In this section, the numerical methods are evaluated using more quantitative approaches.

7.1 Quasi-static pressure

The time-varying average overpressure in the chamber can be extracted from the numerical results through output of the volume-integrated pressure in the computational domain. At late times, this average overpressure approaches the chamber quasi-static pressure. Experimental values are determined by averaging the QSP values measured at the five gauge locations. Quasi-static pressure estimates were also obtained using the Cheetah constant-volume explosion analysis, which assumes perfect mixing of detonation products and air. Because perfect mixing is not present in either the experiments or the numerical simulations, the QSP values for these cases must be lower than Cheetah predictions.

The QSP results for the baseline JWL/CEA simulations (Fig. 9) are obviously erroneous as they exceed both the experimental and Cheetah predictions. While the addition of the Afterburning EOS does reduce the error in the QSP prediction, the final combination of the Afterburning EOS with the Variable-Gamma EOS for air results in extremely good agreement with the experimental data. This excellent agreement carries forward to the simulations involving the other charge masses as well (Fig. 10).

7.2 Transient solution comparison

A method was derived to quantitatively determine the agreement between experimental and numerical waveforms both in terms of shock magnitudes and times of arrival. An average overpressure error, $\overline{P_{\text{error}}}$, is computed for each numerical gauge as:

$$\overline{P_{\text{error}}} = \frac{\sum_{n=0}^{n_{\text{pts}}} \left| P_n^{\text{exp}} - P_n^{\text{sim}} \right|}{n_{\text{pts}}}, \tag{9}$$

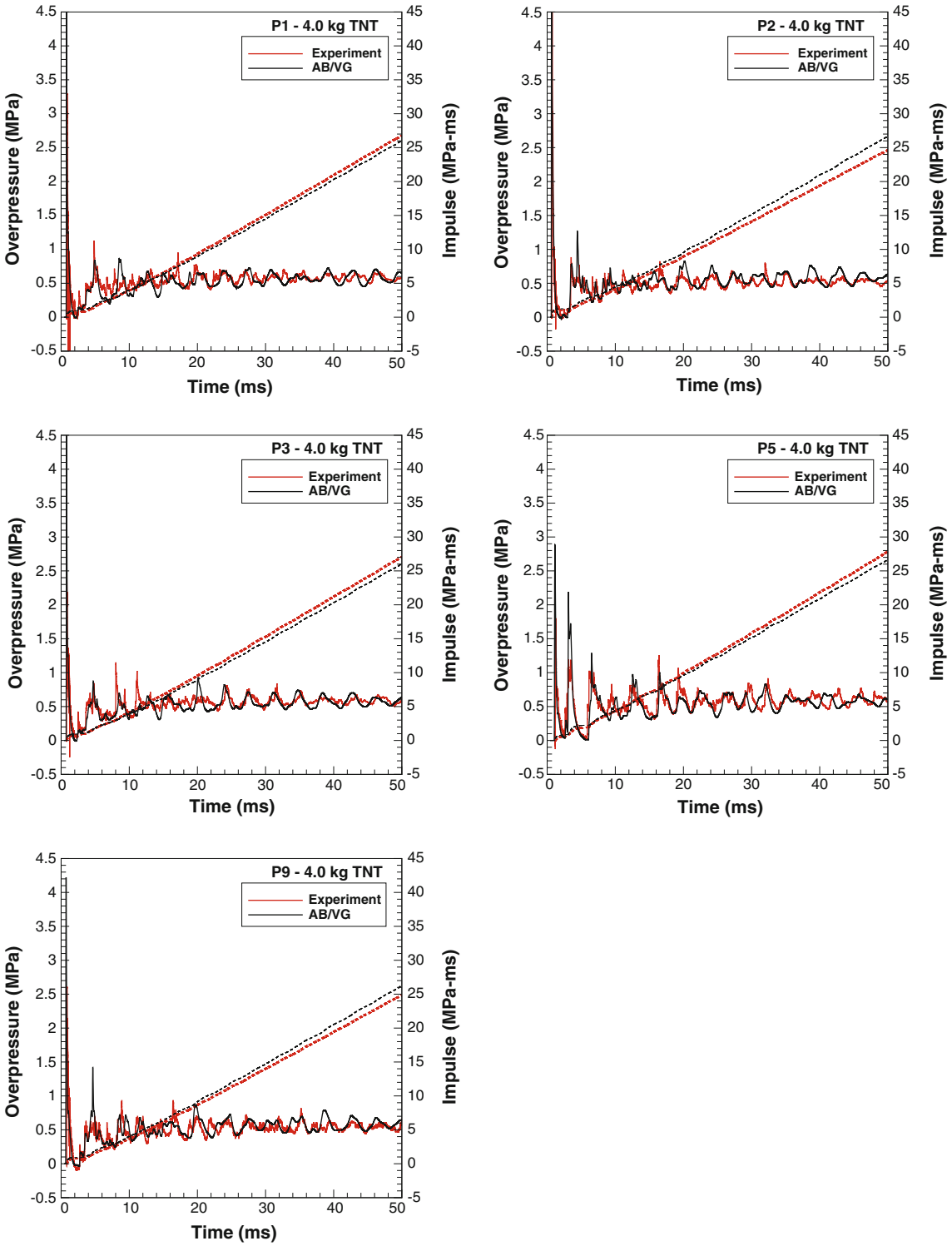

Fig. 7 Comparison of simulation results (AB/VG) using Variable-Gamma EOS for air and simplified mixing model with experiment for 4.0 kg TNT scenario (*solid lines* pressure, *dashed lines* impulse)

where P_n^{exp} is the experimental pressure at a point in time, n, and P_n^{sim} is the numerical pressure at the same point in time. A summation is taken over all points, n_{pts}, within a specific time range. A $\overline{P_{\text{error}}}$ factor of zero indicates perfect agreement. While experimental pressure measurements are recorded at a fixed frequency (1 MHz), the output frequency of the numerical data varies with the computational timestep. To use Eq. 9 to analyze the data,

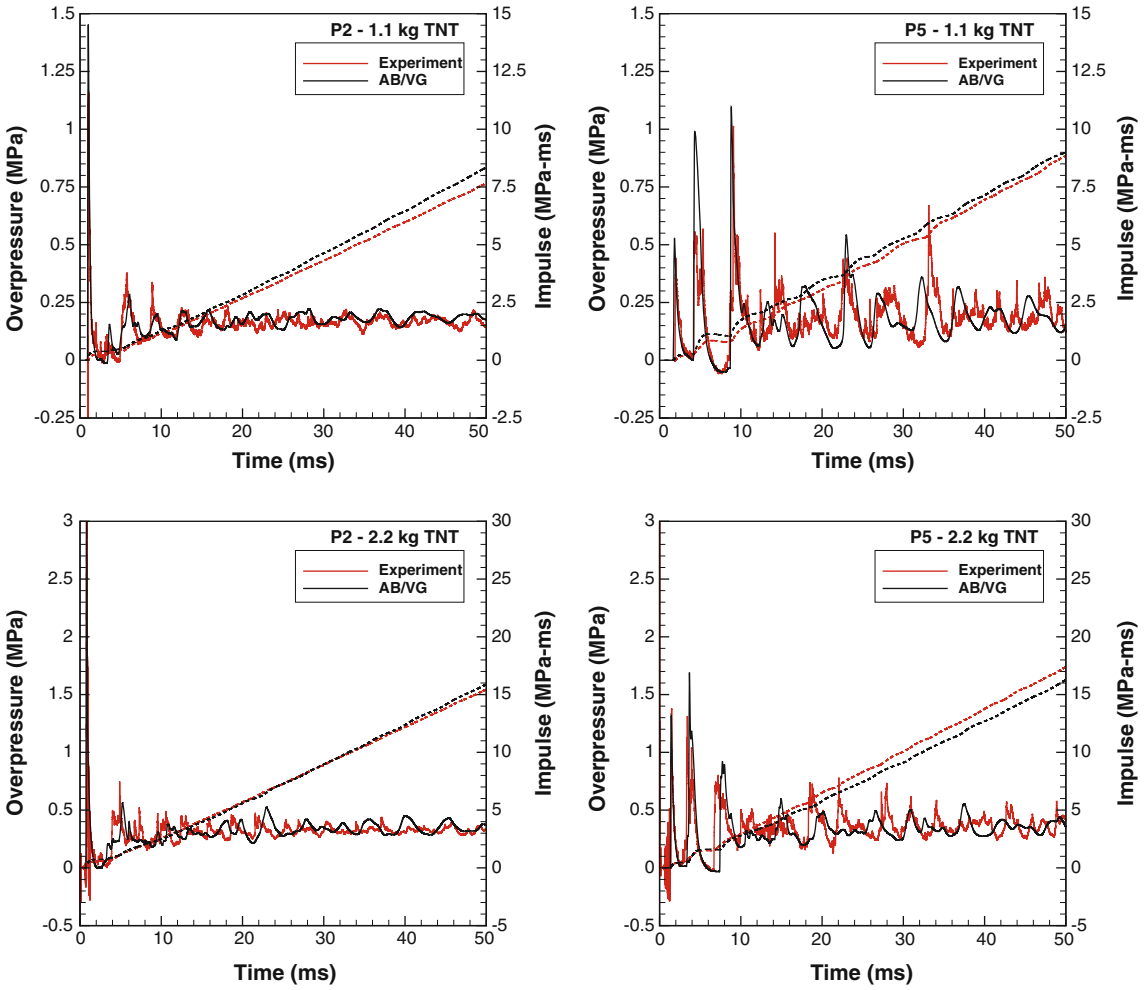

Fig. 8 Select results using AB/VG EOS combination for other TNT masses: *top* 1.1 kg, *bottom* 2.2 kg (*solid lines* pressure, *dashed lines* impulse)

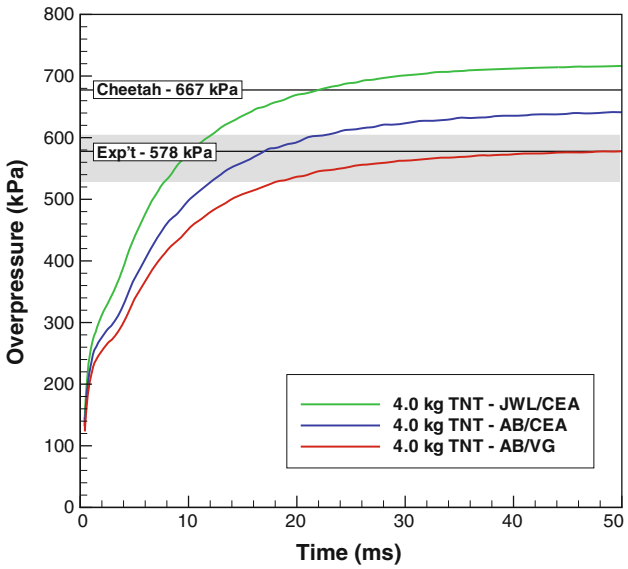

Fig. 9 Effect of equation of state on quasi-static pressure measurements/results for 4.0 kg explosive. *Grey band* surrounding experimental QSP value shows range in experimental gauge QSP

the simulation results were first linearly interpolated to create an equivalent pressure history at the experimental output frequency.

The average overpressure error (average $\overline{P_{\text{error}}}$ of the five gauges) was determined for each of the three EOS combinations investigated as compared to experiment (4.0 kg charge). Factors were computed over three different time ranges: very early time (0–2 ms), increasing chamber pressure (2–20 ms), and late-time QSP (20–50 ms), with results given in Table 3. The three EOS combinations noted in Table 3 are: JWL EOS products with Shocked-Air EOS (JWL/CEA); Afterburning EOS (JWL to Variable-Gamma) products with Shocked-Air EOS (AB/CEA); and Afterburning EOS products with Variable-Gamma EOS air (AB/VG).

The average experimental pressure, $\overline{P_{\text{exp}}}$, computed for each gauge is:

$$\overline{P_{\text{exp}}} = \frac{\sum_{n=0}^{n_{\text{pts}}} \left| P_n^{\text{exp}} \right|}{n_{\text{pts}}} \tag{10}$$

and Table 3 gives the averaged $\overline{P_{\text{exp}}}$ for the five experimental gauges in each of the three time ranges. The average exper-

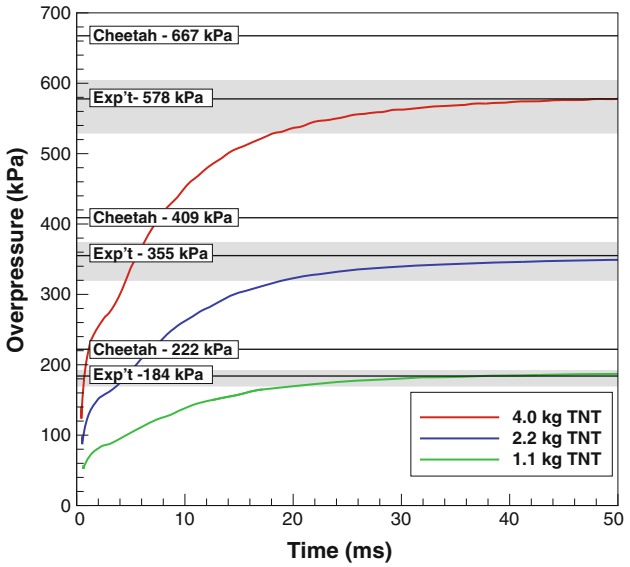

Fig. 10 Effect of charge mass on quasi-static pressure measurements/results for Afterburning EOS with Variable Gamma EOS air. *Grey band* surrounding experimental QSP value shows range in experimental gauge QSP

imental pressure is high in the very early time and is dominated by the high incident shock. The average pressure then drops in the 2–20 ms period, due to smaller shock magnitudes during chamber pressurization. Finally, the average experimental pressure approaches the QSP value in the late time.

The percentage values given in brackets represent the difference in the pressure error as compared to the average experimental pressure in the same time range. In all cases, the largest numerical errors were observed in the very early time. This timeframe contains the largest pressure magnitudes and, therefore, differences in wave arrival times have a very large influence on the error. Overall wave magnitudes are far lower at late times, resulting in much lower error values even when QSP values may differ. Based on this analysis, incorporation of the Afterburning/Variable-Gamma EOS combination gave a slight improvement in the very early time results, with a significant reduction in the error ($\sim 40-50\%$) at all later times when compared to the baseline approach. The relatively low average pressure errors in this time range are also consistent with the qualitative findings.

8 Additional results

Pressure was not the only flow/thermodynamic property to be analyzed. The following sections give some additional results of interest. All simulation results are from the Afterburning EOS/Variable-Gamma EOS combination.

8.1 Comparison to quasi-static temperature

Although somewhat limited in scope, temperature measurements were recorded for each trial. Experimental temperatures were obtained using a local pyrometric sensor at the location given in Fig. 1 based on two wavelengths (690 and 568 nm) [5].

Figure 11 illustrates temperatures from multiple sources for each of the explosive masses considered. Three numerical results are given in each plot: temperature-time histories at the two gauges closest to the experimental pyrometric sensor (P2 and P9), as well as a mass-weighted temperature integrated throughout the entire chamber volume. The experimental measurements and temperatures from the Cheetah constant-volume explosion analysis are also given.

The transient signals in the P2 and P9 numerical gauge histories show some very significant temperature changes, such as at approximately 5 ms in the 2.2 kg case, and at 10 ms in the 1.1 kg case. These large fluctuations in temperature are due to the fireball impinging on the wall gauge positions, and in the 1.1 kg case at 22 ms, the fireball being swept back. There is considerable variation in the temperatures predicted by all sources. At late times (after 40 ms), the numerical temperatures begin to approach the Cheetah equilibrium values. The local temperatures near the chamber wall computed at P2 and P9 are higher than the Cheetah results since shock reflections between the chamber wall and the fireball interface not only increase pressures but also temperature due to enhanced local mixing. On the other hand, the volume-averaged numerical temperature is lower than the Cheetah values resulting from the overall reduction in the extent of mixing and combustion. Considering that it takes much longer time to achieve temperature equilibrium than pressure equilibrium, the unsteady temperature at 50 ms has not yet reached the equilibrium or quasi-static value, particularly for the larger explosive charges.

Table 3 Computed average of five gauge pressure errors for EOS combinations (4.0 kg TNT)

Time range (ms)	$\overline{P_{\text{exp}}}$ (kPa)	Average overpressure error (kPa) (% diff to exp. average pressure)		
		JWL/CEA (%)	AB/CEA (%)	AB/VG (%)
0–2	484.4	484.5 (100)	440.9 (91)	381.1 (78)
2–20	475.2	172.1 (36)	121.0 (25)	101.7 (21)
20–50	564.6	153.7 (27)	107.1 (19)	70.6 (13)

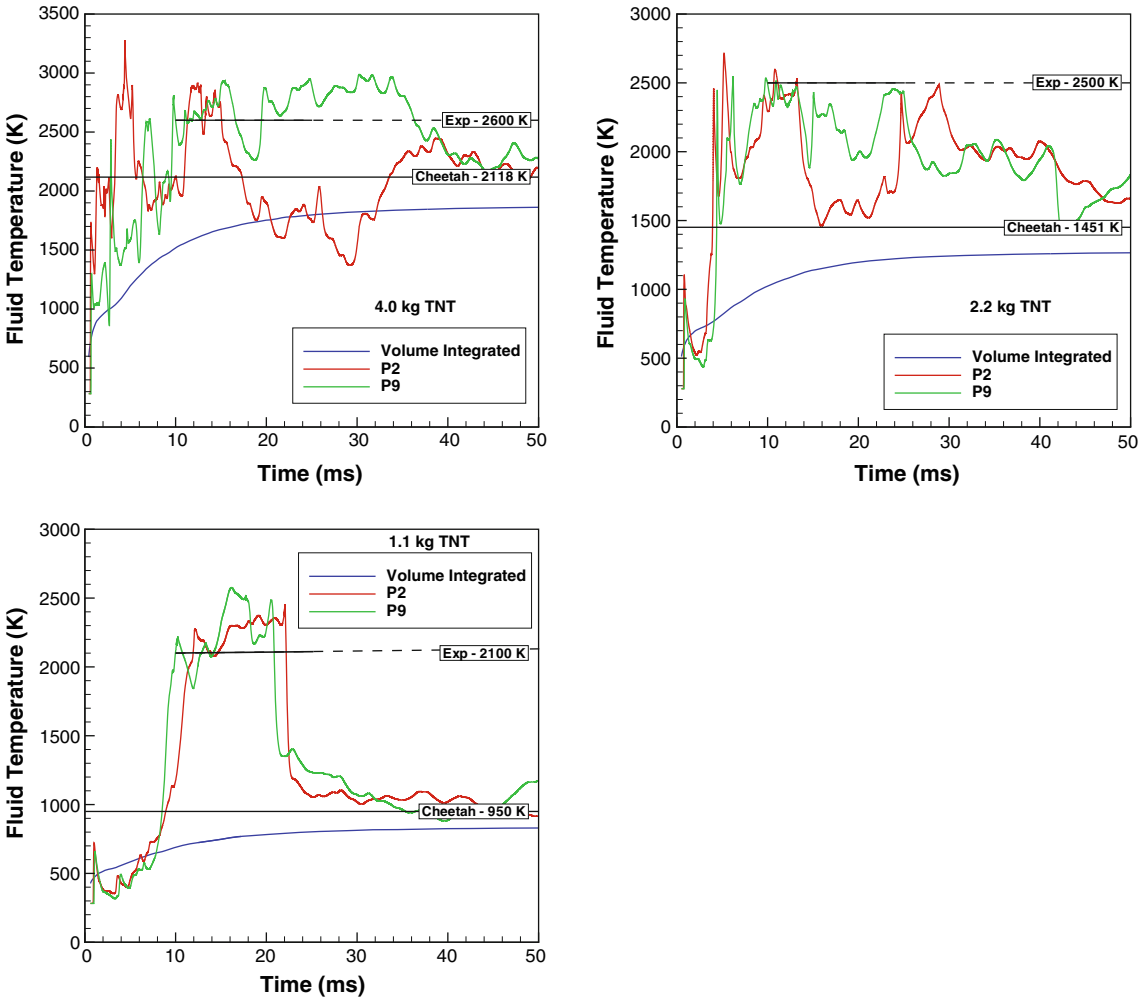

Fig. 11 Wall temperature histories (P2, P9 Gauges), volume-integrated temperature history, experimental temperature measurements and Cheetah CV equilibrium temperatures for 4.0, 2.2 and 1.1 kg charges

Overall, there is reasonable agreement between the Cheetah equilibrium and numerical results considering that some degree of difference is expected due to the assumption of perfect mixing in the Cheetah case. However, there are significant differences between the numerical results and experimental measurements. This discrepancy may be attributed to two aspects. First, pyrometry measurements are based on radiation from particle sources including carbon and other particles in the chamber. In general, such measurements show a difference of hundreds of degrees with respect to fluid temperature. Secondly, the experimental data shown in Fig. 11 are the average temperatures between 10 and 25 ms. After 25 ms, the noise-to-signal ratio becomes too significant to make physical measurements meaningful. The transient measurement of near-field explosion fluid temperature remains as an unresolved challenging technological issue.

8.2 Spatial/temporal variation in specific heat ratio

A benefit of numerical modelling is the ability to extract properties which are not measurable experimentally. Figure 12 plots the variation in specific heat ratio (gamma) at three gauge locations for the 4.0 kg TNT scenario. Also shown is the value computed by the Cheetah constant-volume explosion analysis. Considering the equations of state used in the baseline simulations, the specific heat ratio ranges between 1.3 (detonation products) and 1.4 (air). However, by accounting for variations in products composition, a range in specific ratio of 1.2–1.4 is found. Towards the simulation end time, all gauges approach a constant value which is slightly greater than the Cheetah value. This is expected as, again, the Cheetah simulation represents a condition of perfectly mixed products and air which is not found in the simulations/experiment.

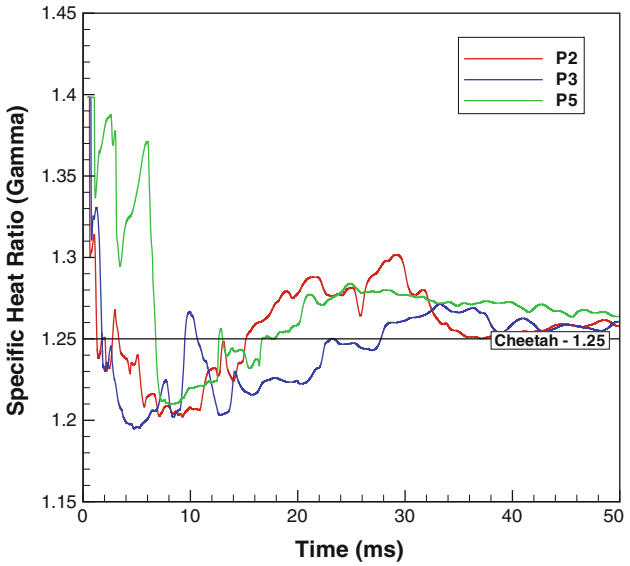

Fig. 12 Computed specific heat ratio (AB/Variable-Gamma EOS combination) compared with Cheetah constant-volume value. Wall measurements at three gauges (P2, P3, P5) for 4.0 kg TNT scenario

9 Conclusions

Numerical afterburning investigations were completed using CFD methods. The primary objective was to investigate the influence of the detonation products EOS on the prediction of the efficiency of TNT afterburning and the times of arrival and magnitudes of reverberating shock waves in a closed chamber. A new EOS was proposed, denoted the Afterburning EOS. This EOS employs a combination of methods, using the JWL EOS in the high-pressure regime and transitioning to a Variable-Gamma EOS at lower pressures.

Simulations of 1.1, 2.2 and 4.0 kg TNT charges suspended in a closed explosion chamber were performed using both existing methods and the new Afterburning EOS. It was found that the Afterburning EOS gave better agreement with the experimental measurements in the early to mid time. In the late time, the Afterburning EOS resulted in better agreement in quasi-static pressure; however, the agreement with the transient late time signals could be improved. Overall simulation run times were approximately 9% longer than the JWL/CEA combination, largely because of the necessity of computing one extra specie equation (N_2).

Excellent transient and quasi-static agreement was obtained using the Afterburning EOS in combination with the VG EOS for air with a simplified mixing model applied automatically and when possible. Simulation run times using this approach were approximately 13% shorter than the JWL/CEA combination, despite requiring solution of one extra governing equation and a more computationally-expensive EOS algorithm. This EOS combination is recommended for future studies involving afterburning explosives, particularly in semi- and fully-confined environments where the contribution of afterburning to the structural loading can be significant.

All simulations in this study focused on single-phase, uncased calculations. Although carbon in the detonation products is in solid form, the assumption was made that it is in mechanical and thermal equilibrium with the gas. Modelling carbon as solid particles may be more physically accurate; however, significant extra computational effort is required to perform multi-phase calculations. The presence of casing is not expected to affect the Afterburning EOS approach and the method is compatible with a range of other physical and numerical models.

The methods described here have been used for explosions of various masses of C4 explosive in the same chamber, and the numerical results showed the same confidence in comparison with experiments [12]. Future work will focus on continuing to apply these methods to the simulation of different explosive formulations and in environments with varying levels of confinement, and refining the algorithm as necessary.

Acknowledgments The authors wish to acknowledge the contributions of several colleagues to this study. Dr. Michael Pegg, Dalhousie University Department of Process Engineering and Applied Science, was a collaborator in the development of the original afterburning equation of state. Mr. Tim Dunbar, Martec Limited, created all of the three-dimensional meshes. This work was funded by Defence R & D Canada-Suffield and Martec Limited.

References

1. Dewey, J.M.: The air velocity in blast waves from TNT explosions. Proc. R. Soc. Lond. A **279**(1378), 366–385 (1964)
2. Baker, W.E.: Explosions in Air. University of Texas Press, Texas (1973)
3. Ornellas, D.L.: Calorimetric determinations of the heat and products of detonation for explosives: October 1961 to April 1982. UCRL-52821. Lawrence Livermore National Laboratory, Livermore (1982)
4. Wolanski, P., Gut, Z., Trzcinski, W.A., Szymanczyk, L., Paszula, J.: Visualization of turbulent combustion of TNT detonation products in a steel vessel. Shock Waves **10**(2), 127–136 (2000)
5. Zhang, F., Anderson, J., Yoshinaka, A.: Post detonation energy release from TNT-aluminum explosives. In: Elert, M., Furnish, M.D., Chau, R., Holmes, N., Nguyen, J. (eds.) Shock Compression in Condensed Matter—2007, vol. CP955, pp. 885–888. American Institute of Physics, Melville (2007)
6. Kuhl A.L., Forbes, J., Chaudler, J., Oppenheim, A.K., Spektor, R., Ferguson, R.E.: Confined combustion of TNT explosion products in air. UCRL-JC-131748. Lawrence Livermore National Laboratory, Livermore (1998)
7. Kuhl, A.L., Howard, M., Fried, L.: Thermodynamic model of afterburning in explosions. In: Proceedings of 34th International ICT Conference: Energetic Materials: Reactions of Propellants, Explosives, and Pyrotechnics, Karlsruhe, Germany, June 24–27 (2003)
8. Bell, J.B., Day, M., Beckner, V., Rendleman, C., Kuhl, A., Neuwald, P.: Numerical simulation of the combustion of PETN/TNT products

with air in closed chambers. In: Proceedings of 20th International Colloquium on the Dynamics of Explosions and Reactive Systems, Montreal, Canada, July 31–August 5 (2005)
9. Ames, R.G., Drotar, J.T., Silber, J., Sambrook, J.: Quantitative distinction between detonation and afterburn energy deposition using pressure-time histories in enclosed explosions. In: Proceedings of 13th International Detonation Symposium, Norfolk, VA, July 23–28 (2006)
10. Ripley, R.C., Donahue, L., Dunbar, T.E., Zhang, F.: Explosion performance of aluminized TNT in a chamber. In: Proceedings of 19th International Symposium on the Military Aspects of Blast and Shock, Calgary, Canada, October 1–6 (2006)
11. Donahue, L., Pegg, M., Zhang, F.: Afterburning of TNT detonation products in air. In: Proceedings of 7th International Symposium on Hazards, Prevention, and Mitigation of Industrial Explosions, St. Petersburg, Russia, July 7–11 (2008)
12. Donahue, L.: Afterburning of TNT Detonation Products in Air. M.A.Sc. thesis, Dalhousie University, Halifax, Canada (2009)
13. Anderson, J.D.: Computational Fluid Dynamics: The Basics with Applications. McGraw-Hill Inc., Toronto (1995)
14. Batten, P., Clarke, N., Lambert, C., Causon, D.M.: On the choice of wavespeeds for the HLLC Riemann solver. SIAM J. Sci. Comput. **18**(6), 1553–1570 (1997)
15. Benson, D.J.: Computational methods in Lagrangian and Eulerian hydrocodes. Comput. Methods Appl. Mech. Eng. **99**, 235–394 (1992)
16. Mader, C.L.: Numerical Modeling of Explosives and Propellants, 2nd edn. CRC Press, Boca Raton (1998)
17. Lee, E. L., Hornig, H. C., Kury, J. W.: Adiabatic expansion of high explosive detonation products. UCRL-50422. Lawrence Radiation Laboratory, Livermore (1968)
18. Jones, H., Miller, A.R.: The detonation of solid explosives: The equilibrium conditions in the detonation wave-front and the adiabatic expansion of the products of detonation. Proc. R. Soc. Lond. A **194**(1039), 480–507 (1948)
19. Wilkins, M.L.: The equation of state of PBX 9404 and LX04-01. UCRL-7797. Lawrence Radiation Laboratory, Livermore (1964)
20. Fickett, W., Davis, W.C.: Detonation. University of California Press, Berkeley (1979)
21. Dobratz, B. M., Crawford, P. C.: Properties of chemical explosives and explosive simulants. UCRL-51319. Lawrence Radiation Laboratory, Livermore (1974)
22. Fried, L.E., Howard, W.M., Souers, P.C.: CHEETAH 2.0 User's Manual. UCRL-MA-117541 Rev. 5. Lawrence Livermore National Laboratory, Livermore (1998)
23. Bastea, S., Fried, L.E.: Chemical equilibrium detonation. In: Zhang, F. (ed.) Detonation Dynamics, pp. 1–31. Springer, Berlin (2012)
24. Souers, P.C., Forbes, J.W., Fried, L.E., Howard, W.M., Anderson, S., Dawson, S., Vitello, P., Garza, R.: Detonation energies from the cylinder test and CHEETAH V3.0. Propellants Explos. Pyrotech. **26**(4), 180–190 (2001)
25. Leadbetter, J., Ripley, R.C., Zhang, F., Frost, D.L.: Multiple energy scaling of blast waves from heterogeneous explosives. In: Proceedings of 21st International Colloquium on the Dynamics of Energetic and Reactive Systems, Poitiers, France, July 23–27 (2007)
26. Gordon, S., McBride, B.J.: Computer program for calculation of complex chemical equilibrium compositions and applications. NASA Reference, Publication 1311 (1994)